axioms

MDPI

Article

Wavelet Energy Entropy for Predictability and Cross-Market Similarity in Crude Oil Benchmarks

Maria Carannante [1] and Alessandro Mazzoccoli [2,*]

[1] Department of Human Sciences, Link Campus University, Via del Casale di San Pio V, 00165 Rome, Italy; m.carannante@unilink.it
[2] Department of Economics, Roma Tre University, Via Silvio D'Amico 77, 00145 Rome, Italy
* Correspondence: alessandro.mazzoccoli@uniroma3.it

Abstract

We study the predictability and cross-market structural similarity of Brent, WTI, and Dubai crude oil futures by means of a wavelet-based Sharma–Mittal energy entropy measure. The proposed framework combines multiresolution wavelet decomposition with a parametric generalised entropy, allowing the characterisation of informational complexity across scales and entropic parameters. We show that predictability is jointly scale- and parameter-dependent. Despite this dependence, the resulting wavelet entropy surfaces exhibit a high degree of geometric similarity across the three benchmarks. A discrepancy analysis further indicates that cross-market differences are localised in restricted regions of the parameter space, whereas intermediate scales are associated with maximal entropy values. Outside such regions, the entropy surfaces converge. Overall, the results provide evidence of a common multi-scale entropic structure underlying crude oil benchmarks, with regional effects affecting predictability without altering the global structural properties. These findings are consistent with the hypothesis of strong informational integration in global oil markets.

Keywords: wavelet analysis; entropy; financial applications

MSC: 42C40; 46E30; 94A17

1. Introduction

Energy markets play a central role in the global economy, strongly affecting industrial activity, trade flows, and economic policy decisions. Within this framework, crude oil represents one of the most important energy sources and one of the most actively traded financial assets at the global level. Among the available benchmarks, Brent, West Texas Intermediate (WTI), and Dubai Crude Oil are the main references for determining oil prices in the major geographic markets, namely Europe, North America, and Asia, respectively. Crude oil price variations can arise from various causes, including global supply disruptions, shifts in global demand, and regional factors, each with distinct macroeconomic consequences [1]. Understanding these causes is crucial to interpreting price dynamics and benchmark differentials across markets.

WTI is the benchmark price for crude oil produced in the United States and is traded on the New York Mercantile Exchange, with physical delivery in Cushing, Oklahoma, a major logistics and pricing hub connecting crude oil supplies to refineries on the U.S. Gulf Coast [2]. Brent crude, extracted in the North Sea and composed of a blend of four crude

Academic Editors: Conghua Wen, Yi Hong, Xianming Sun, Fei Ma and Maria Letizia Guerra

Received: 20 February 2026
Revised: 20 March 2026
Accepted: 27 March 2026
Published: 28 March 2026

streams (Brent, Forties, Oseberg, and Ekofisk), is traded on the Intercontinental Exchange and delivered to the Sullom Voe terminal. It is important to note that Brent is the pricing benchmark for approximately two-thirds of the crude oil traded globally. Dubai crude, often referred to as Dubai/Oman in pricing formulas, is a medium-sour crude produced in the Middle East and is the primary benchmark for crude oil exports from the Persian Gulf to Asian markets. Unlike Brent and WTI, Dubai crude is traded primarily in the over-the-counter market and plays a crucial role in pricing long-term supply contracts for Asia [3].

These benchmarks differ not only in their geographical relevance and trading mechanisms but also in their physical characteristics. WTI and Brent are light and low-sulphur crude oils, with API gravities of 39.6 and 38.6 degrees and sulphur contents of 0.24% and 0.37%, respectively [4]. In contrast, Dubai crude is heavier and more sulphur-intensive, with an API gravity of approximately 31 degrees and a sulphur content close to 2% [5]. Such differences contribute to persistent price differentials and heterogeneous market dynamics across benchmarks.

Although the empirical literature has traditionally focused on Brent and WTI, a growing number of studies have started to investigate the dynamics of the Dubai crude benchmark, emphasising its relevance in the price formation process of Middle Eastern crude oil exports to Asia and reporting distinctive statistical properties linked to regional demand conditions, pricing formulas, and OPEC supply strategies. For instance, Mann and Sephton [6] document long-run relationships and dynamic interactions among major crude oil benchmarks such as WTI, Brent and Oman, highlighting the strong integration of global oil markets and the role of Middle Eastern benchmarks in the pricing system. Furthermore, the major crude oil markets exhibit interconnected price dynamics and global time-varying spillovers, highlighting structural patterns of co-movement and volatility persistence [7].

The price dynamics of Brent, WTI, and Dubai arise from a complex interaction between physical and financial factors, including global supply and demand conditions, geopolitical tensions, OPEC decisions, technological innovations, and speculative activity. As a result, future price time series exhibit several stylised facts commonly observed in financial markets, such as high volatility, volatility clustering, non-linear dependence, and possible structural breaks. As a consequence, investigating the common structure of major crude oil benchmarks is a crucial issue for predictability and market efficiency.

A significant body of the literature has examined the predictability of crude oil prices, with a particular focus on the Brent and WTI benchmarks, although a growing literature has emerged in recent years regarding Dubai crude prices.

In this context, predictability plays a central role in risk and data analysis, as this refers to the extent to which future prices or market dynamics can be inferred from past observations. The accuracy of such forecasts depends on several factors, including the intrinsic properties of the data, the quality and reliability of the available information, and the analytical methodologies employed.

Pioneering studies have primarily investigated market efficiency conditions using linear econometric tools, such as variance ratio tests, generally finding limited evidence of return predictability and supporting the weak-form efficient market hypothesis (e.g., [8]). More recent contributions, however, suggest that crude oil market efficiency varies over time, with episodic predictability driven by specific market conditions [9]. There are also robust results describing the relationship between WTI and Brent. WTI has historically played a dominant role in determining global oil prices, particularly in high-frequency data and even when the market diverges from Brent crude [10]. In contrast, a limited number of studies explicitly focus on Dubai crude; emerging evidence suggests that this benchmark

may have its own patterns of predictability, driven by regional market structures and exposure to OPEC pricing mechanisms.

In parallel, several studies have highlighted the role of non-linear dynamics and the study of higher-order moments in crude oil prices, documenting that, although returns themselves are often difficult to predict, volatility measures exhibit predictable persistence. Using a variety of approaches, including GARCH family models, stochastic volatility specifications, non-parametric causality frameworks, and machine learning techniques, these studies provide evidence of significant predictability of crude oil price volatility across major benchmarks [11,12]. From an investor's perspective, these findings have important implications for risk management, hedging, and portfolio allocation in crude oil markets [13].

More recent contributions highlight how crude oil price dynamics are characterized by non-linear dependence, regime shifts, and multi-scale time structures, which cannot be fully captured by traditional linear models in econometrics. In this context, distance-based approaches such as Dynamic Time Warping (DTW) have been introduced to analyse similarities and co-movements between Brent and WTI oil price series, accounting for time mismatches and asynchronous dynamics [14]. DTW provides a more flexible representation of the evolving relationship between major oil benchmarks. Further analyses indicate the existence of common speculative bubbles in WTI, Brent, and Dubai oil prices, characterized by simultaneous explosive effects that were notably observed during the 1986 and 2008 crises [15]. This was achieved using the double-recursion algorithm, specifically developed for bubble detection, which allows for the more accurate identification and dating of exuberant price dynamics than traditional approaches [16].

Furthermore, the literature has increasingly incorporated Machine Learning techniques to enhance forecasting performance and uncover complex non-linear patterns in oil price volatility dynamics [17–19]. Simultaneously, information–theoretic and multi-scale methodologies, most notably wavelet entropy–based predictability measures, have been increasingly applied to crude oil prices to capture the impact of fluctuations, price spikes, and rare events [20]. By decomposing price dynamics across different time horizons, multi-scale approaches offer valuable insights into the persistence and structure of predictable components across benchmarks. Recent evidence further suggests that wavelet entropy and complexity–entropy curve frameworks are particularly effective in assessing crude oil price predictability during periods marked by heightened uncertainty and long-term structural transformations in global oil markets [21,22].

In this study, we apply the Wavelet Sharma–Mittal Energy Entropy measure, introduced by [23], to analyse the predictability of Brent, WTI, and Dubai crude oil prices.

While the co-movement and common characteristics of crude oil markets are typically investigated using classical entropy measures or single-scale approaches, the integration of wavelet decomposition with the Sharma–Mittal entropy framework allows for a multi-scale assessment of uncertainty. This approach provides a more nuanced understanding of price dynamics across different frequencies and captures complex patterns in market behaviour that conventional methods may overlook.

Accordingly, the study addresses the following research questions:

RQ1: How does predictability of Brent, WTI, and Dubai crude oil futures vary across different time scales and entropy parameters?
RQ2: Do the three benchmarks exhibit similar multi-scale entropy surface geometries?
RQ3: How is cross-market predictability affected by period of market shocks?

For these reasons, the Wavelet Sharma–Mittal energy entropy framework offers new insights into the short- and long-run predictability of major crude oil benchmarks.

The paper is organized as follows. Section 1 provides the introduction and the motivation for our analysis. Section 2 presents the methodology, while Section 3 describes the data used. Section 4 reports and discusses the results. Finally, Section 5 concludes.

2. Methodology

2.1. Wavelet Representation

A continuous signal is modeled as a function $f \in L^2(\mathbb{R})$, with the space of square-integrable functions defined as $L^2(A) = \{\phi : \int_A |\phi(x)|^2 dx < \infty\}$. Wavelet analysis represents f by dilations and translations of a function w, defined as

$$w_{a,b}(x) = |a|^{-1/2} w\left(\frac{x-b}{a}\right), \quad a \neq 0,\ b \in \mathbb{R}. \tag{1}$$

In particular, under the standard framework of orthogonal multiresolution analysis (MRA), a function $w \in L^2(\mathbb{R})$ is called a mother wavelet if the family

$$w_{s,n}(x) = 2^{s/2} w(2^s x - n), \qquad s, n \in \mathbb{Z}, \tag{2}$$

forms an orthonormal basis of $L^2(\mathbb{R})$, where $s \in \mathbb{Z}$ represents the scale and $n \in \mathbb{Z}$ the translation parameter.

Orthonormality follows from two key properties of the MRA construction: (i) the orthogonality of the integer translations of the wavelet within each resolution level, and (ii) the mutual orthogonality of detail subspaces W_s across different scales, i.e., $W_s \perp W_{s'}$ for $s \neq s'$. Completeness is guaranteed by the direct sum decomposition

$$L^2(\mathbb{R}) = \overline{\bigoplus_{s \in \mathbb{Z}} W_s},$$

which ensures that any square–integrable function can be represented as a superposition of wavelet components across all scales and locations.

Consequently, for any $f \in L^2(\mathbb{R})$, the associated wavelet coefficients are defined as

$$c_{s,n} = \langle f, w_{s,n} \rangle,$$

and the function admits the expansion

$$f(x) = \sum_{s \in \mathbb{Z}} \sum_{n \in \mathbb{Z}} c_{s,n}\, w_{s,n}(x),$$

where the series converges in the L^2 sense, see for other details [24–28].

In particular, in our analysis, we employ the Haar wavelet as the mother wavelet. The Haar wavelet is the simplest orthogonal wavelet and is defined by the wavelet function

$$w_{Haar}(x) = \begin{cases} 1 & 0 \leq x < \frac{1}{2}, \\ -1 & \frac{1}{2} \leq x < 1, \\ 0 & \text{otherwise.} \end{cases}$$

The corresponding wavelet family is obtained through the dyadic dilations and translations introduced in Equation (2). The Haar wavelet was selected for its simplicity and its ability to capture local variations and abrupt changes in the signal. Moreover, its orthogonality allows for a clear separation of the signal energy across different scales, which is particularly suitable for the multiscale entropy analysis considered in this work.

2.2. Entropies and the Sharma–Mittal Entropy

Entropy provides a quantitative measure of the uncertainty associated with a discrete probability distribution $\mathbf{p} = \{p_1, \ldots, p_n\}$, with $p_i \geq 0$ and $\sum_{i=1}^{n} p_i = 1$. Among the various entropy measures proposed in the literature, the Sharma–Mittal entropy plays a central role as a two-parameter generalization encompassing several classical entropies.

The Sharma–Mittal entropy is defined, for $\alpha, \beta \in \mathbb{R}^+ \setminus \{1\}$, $\alpha \neq \beta$, as

$$H^{\mathrm{SM}}_{\alpha,\beta}(\mathbf{p}) = \frac{1}{\beta - 1}\left[\left(\sum_{i=1}^{n} p_i^{\alpha}\right)^{\frac{\beta-1}{\alpha-1}} - 1\right]. \tag{3}$$

This formulation provides a unified framework for entropy-based measures of uncertainty.

Well-known entropy measures arise for particular cases of the Sharma–Mittal entropy. In the limit $\beta \to 1$, it reduces to the Rényi entropy

$$\lim_{\beta \to 1} H^{\mathrm{SM}}_{\alpha,\beta}(\mathbf{p}) = H^{\mathrm{R}}_{\alpha}(\mathbf{p})$$

where $H^{\mathrm{R}}_{\alpha}(\mathbf{p})$ is defined as

$$H^{\mathrm{R}}_{\alpha}(\mathbf{p}) = \frac{1}{1 - \alpha} \log\left(\sum_{i=1}^{n} p_i^{\alpha}\right), \tag{4}$$

which preserves additivity and is widely used in information theory and multifractal analysis.

When $\beta = \alpha$, the Sharma–Mittal entropy coincides with the Tsallis entropy

$$H^{\mathrm{T}}_{\alpha}(\mathbf{p}) = \frac{1}{\alpha - 1}\left(1 - \sum_{i=1}^{n} p_i^{\alpha}\right), \tag{5}$$

a non-additive entropy suitable for the description of non-extensive systems.

Finally, in the limit $\alpha \to 1$ and $\beta \to 1$, both Rényi and Tsallis entropies, and consequently the Sharma–Mittal entropy, converge to the classical Shannon entropy

$$\lim_{(\alpha,\beta) \to (1,1)} H^{\mathrm{SM}}_{\alpha,\beta}(\mathbf{p}) = H(\mathbf{p})$$

where $H(\mathbf{p})$ is defined as

$$H(\mathbf{p}) = -\sum_{i=1}^{n} p_i \log p_i. \tag{6}$$

Therefore, the Sharma–Mittal entropy can be regarded as a comprehensive generalization that unifies Shannon, Rényi, and Tsallis entropies within a single parametric framework; for further details, see the paper by [29–31].

2.3. Wavelet Sharma–Mittal Entropy

Given a signal $f \in L^2(\mathbb{R})$, the total energy is defined as

$$E(f) = \int_{\mathbb{R}} |f(x)|^2 \, dx.$$

Using a discrete wavelet transform, f can be expanded in terms of a set of wavelet basis functions $\{w_{s,n}\}_{s \in \mathcal{S}, n \in \mathbb{Z}}$:

$$f(x) = \sum_{s \in \mathcal{S}} \sum_{n \in \mathbb{Z}} c_{s,n} \, w_{s,n}(x),$$

where $c_{s,n} = \langle f, w_{s,n} \rangle$ are the wavelet coefficients.

Thanks to the orthonormality of the wavelet basis, the energy of the signal can be expressed in terms of the wavelet coefficients as

$$E(f) = \sum_{s \in \mathcal{S}} \sum_{n \in \mathbb{Z}} |c_{s,n}|^2,$$

where $\mathcal{S}$ denotes the set of admissible scales, with cardinality $S := |\mathcal{S}| = \lfloor \log_2(N) \rfloor$ if the signal has length N.

Fixing the energy at a given scale s, we define

$$E_s(f) = \sum_{n \in \mathbb{Z}} |c_{s,n}|^2.$$

The *relative energy at scale s* is then naturally defined as

$$p_s = \frac{E_s(f)}{E(f)},$$

so that $\sum_{s \in \mathcal{S}} p_s = 1$. This allows one to interpret $\{p_s\}_{s \in \mathcal{S}}$ as a probability distribution across scales, which is useful for defining entropy-based measures of signal complexity.

Based on this energy-based probability distribution, the wavelet energy complexity of the signal can be quantified through the Sharma–Mittal entropy

$$H^{\mathrm{SM}}_{\alpha,\beta}(f) = \frac{1}{\beta - 1} \left[\left(\sum_{s \in \mathcal{S}} p_s^{\alpha} \right)^{\frac{\beta-1}{\alpha-1}} - 1 \right], \qquad \alpha, \beta \in \mathbb{R}^+ \setminus \{1\},\ \alpha \neq \beta \tag{7}$$

The parameter α controls how the probability is adjusted or weighted in the entropy calculation, while β determines the degree to which the entropy is additive for independent systems. The first parameter, α, sets the weighting for different events, controlling how sensitive the entropy measure is to the probability distribution. The second parameter, β, manages how these weights are combined. Essentially, the parameter β defines the additive transformation, changing the type of mean, such as arithmetic or geometric, used to combine the weighted contributions of individual states. By changing α, one can adjust the focus on events with different probabilities. When α is greater than 1, more weight is given to more probable events, while when α is less than 1, the focus shifts to rarer events. As a result, the parameter α effectively adjusts the deformation of the probability moment.

2.4. Wavelet Sharma–Mittal Energy Entropy Measure

Thanks to the mathematical formulation of the wavelet Sharma–Mittal entropy defined in Equation (7), the wavelet Sharma–Mittal energy entropy measure is defined as follows:

$$\begin{aligned} &WSEEM_{\alpha,\beta} : L^2(\mathbb{R}) \times (\mathbb{R}^+ \setminus \{1\})^2 \to [0,1) \\ &WSEEM_{\alpha,\beta}(f) = 1 - e^{H^{SM}_{\alpha,\beta}(f) - \frac{1}{\beta-1}\left[S^{1-\beta}-1\right]}. \end{aligned} \tag{8}$$

where $\frac{1}{\beta-1}\left[S^{1-\beta} - 1\right]$ is the maximum value reached by the Sharma–Mittal entropy, specifically the value obtained by computing the Sharma–Mittal entropy of a white noise signal (wn); for other details, see [23].

Notably, the following hold:

- If $WSEEM_{\alpha,\beta}$ is close to 1, the entire energy of f is concentrated around a few scales, and thus the time series has high intrinsic predictability, since

$$H^{\mathrm{SM}}_{\alpha,\beta}(wn) \gg H^{\mathrm{SM}}_{\alpha,\beta}(f)$$

  the Sharma–Mittal wavelet entropy of the signal is much lower than the Sharma–Mittal wavelet entropy of the white noise.
- If $WSEEM_{\alpha,\beta}$ is close to 0, the entire energy of f is scattered across all scales (similar to a white noise process) and thus f has very low intrinsic predictability, since

$$H^{\mathrm{SM}}_{\alpha,\beta}(wn) \approx H^{\mathrm{SM}}_{\alpha,\beta}(f).$$

The Sharma–Mittal wavelet entropy of the signal is close to the Sharma–Mittal wavelet entropy of the white noise.

To clarify this concept, we consider two simple examples. Considering $f(x) = c$, $c \in \mathbb{R}$, a constant function, all the energy is concentrated in a single scale s_0, so

$$p_{s_0} = 1, \quad p_s = 0 \text{ for } s \neq s_0.$$

Then,

$$\sum_{s\in\mathcal{S}} p_s^{\alpha} = 1, \quad \text{and thus} \quad H^{\mathrm{SM}}_{\alpha,\beta}(c) = 0.$$

The entropy is zero because all the energy is concentrated in a single scale, so there is no uncertainty in the distribution.

As a consequence,

$$WSEEM_{\alpha,\beta}(c) = 1 - e^{H^{SM}_{\alpha,\beta}(c) - \frac{1}{\beta-1}\left[S^{1-\beta}-1\right]} = 1 - e^{-\frac{1}{\beta-1}\left[S^{1-\beta}-1\right]}.$$

Now, we consider a periodic function, $f(x) = \sin(2\pi kx)$. For simplicity, assume the energy is distributed equally over two dominant scales, s_1 and s_2:

$$p_1 = 0.5, \quad p_2 = 0.5, \quad p_s = 0 \text{ for the other scales.}$$

Then,

$$\sum_{s\in\mathcal{S}} p_s^{\alpha} = (0.5)^{\alpha} + (0.5)^{\alpha} = 2 \cdot (0.5)^{\alpha} = 2^{1-\alpha},$$

and the Sharma–Mittal entropy becomes

$$H^{\mathrm{SM}}_{\alpha,\beta}(\sin(2\pi kx)) = \frac{1}{\beta-1}\left[\left(2^{1-\alpha}\right)^{\frac{\beta-1}{\alpha-1}} - 1\right].$$

The entropy is greater than zero because the energy is distributed across multiple scales, indicating higher uncertainty compared to the constant case, and the associated $WSEEM$ is

$$WSEEM_{\alpha,\beta}(\sin(2\pi kx)) = 1 - e^{H^{SM}_{\alpha,\beta}(\sin(2\pi kx)) - \frac{1}{\beta-1}\left[S^{1-\beta}-1\right]} = 1 - e^{\frac{1}{\beta-1}\left[\left(2^{1-\alpha}\right)^{\frac{\beta-1}{\alpha-1}} - S^{1-\beta}-1\right]}.$$

These examples illustrate how Sharma–Mittal entropy measures the complexity of energy distribution across multiple scales.

3. Data

The analysis is based on WTI, Brent, and Dubai crude oil futures log prices, which represent the main benchmarks of the international oil market. Both series consist of daily data covering the period from April 2014 to January 2026, for a total of 3075 observations, allowing for the inclusion of different phases of the business cycle as well as numerous events relevant to the energy market. The data were retrieved from www.investing.com. April 2014 is the starting date of Dubai futures prices. Prices are expressed in U.S. dollars per barrel. The use of a daily frequency makes it possible to accurately capture short-term price dynamics and the responsiveness of oil prices to economic, geopolitical, and financial shocks. Before the WSEEM estimation, the data were imputed to avoid a huge loss of observations, trying to preserve the multiscale relationships between them. The number of missing observations per series are as follows: Brent—58 missing observations; Dubai–140 missing observations; WTI—4 missing observations. From a qualitative analysis of the missing dates, it is observed that they are not randomly distributed, but occur systematically in clusters associated with market-specific non-trading days. For Brent, whose reference is the UK-based ICE market, missing observations align with UK public holidays (e.g., Good Friday, Early May Bank Holiday, and Boxing Day). In some cases, if the holiday falls on a market closing day, the market remains closed on the following day as well. For WTI, missing points largely correspond to U.S. federal holidays (e.g., Independence Day, Thanksgiving, and Martin Luther King Day), but not all holidays are observed as missing, reflecting partial market closures. In fact, only four missing people were observed from 2014 to 2025. For Dubai, missing observations are more frequent and strongly aligned with both UAE holidays and overlapping US holidays, since Dubai prices are referenced by Platts, which is tied to US futures contracts. For imputations, we choose to use the Kalman filter based on the optimal ARIMA model, selected for each series according to the Akaike information criterion. Unlike naïve methods, such as last observation carried forward or simple linear interpolation, the Kalman filter is a dynamic, model-based approach that explicitly estimates the underlying state of the series. By forecasting missing values based on the persistent dynamics of the series, the Kalman filter preserves the multiscale structure and is expected to introduce less bias across wavelet scales, particularly at intermediate and high frequencies, compared to average or trend imputations. In contrast, restricting the analysis to overlapping trading days avoids imputation but reduces sample size and could introduce bias linked to holidays in the other markets, particularly for Dubai, which is linked to US market through the Platts futures market. For the sake of clarity, for Brent, the selected model is ARIMA(0,1,0) $y_t = y_{t-1} + \varepsilon_t$; for Dubai, it is ARIMA(1,1,1) $y_t = y_{t-1} + 0.96(y_{t-1} - y_{t-2}) + \varepsilon_t + 0.94\varepsilon_{t-1}$; for WTI, it is ARIMA(0,1,4) $y_t = y_{t-1} + \varepsilon_t + 0.02\varepsilon_{t-1} + 0.05\varepsilon_{t-2} + 0.06\varepsilon_{t-3} - 0.04\varepsilon_{t-4}$.

Figure 1 shows the time series of log-prices for the crude oil futures considered.

Figure 1 shows the main crude oil market structural disruptions. The 2014–2015 supply shock can be observed, characterised by a rapid decline. This collapse was triggered by the overproduction of shale oil in the US and OPEC's refusal to cut production to maintain market share. The 2020 pandemic crisis can also be seen, with maximum divergence among oil futures prices. The log-price drops sharply, with a more pronounced decline for WTI with respect to the others. The 2022 geopolitical shock, shows a peak reflecting the risk premium associated with global energy security. The current mean-reverting phase also shows a decrease that indicates a return to historical prices. Overall, the behaviour of the three series reveals key details about their level of integration. Future prices move almost in unison. This result suggest a long-run stationary equilibrium relationship, and the global nature of shocks in crude oil, or, more broadly, energy markets. These results suggest cross-market similarities and common structures, explored further with WSEEM analysis.

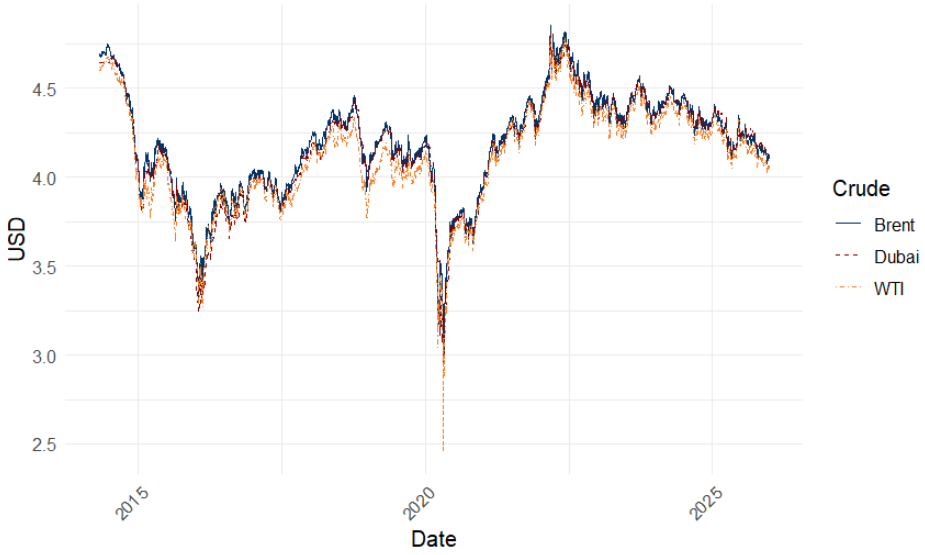

Figure 1. Brent, WTI, and Dubai log-price time series dynamics from April 2014 to January 2026.

4. Results

In this section, we present and discuss the results obtained by applying the WSEEM measure to the futures prices of Brent, WTI, and Dubai crude oil benchmarks.

4.1. Predictability and Cross-Market Similarities in Crude Oil Benchmarks

This section investigates the multi-scale predictability of crude oil futures prices and the degree of similarity across major oil benchmarks by means of the Wavelet Sharma–Mittal Energy Entropy Measure. The analysis is conducted on Brent, WTI, and Dubai futures prices, allowing for a comparative assessment of their multi-scale informational structure.

The wavelet decomposition was implemented in R 4.5.2 using the `wavelets` package. We employed the DWT with the Haar wavelet as the mother wavelet, and the boundary effects were handled through periodic extension of the signal, which corresponds to the default boundary treatment in the implementation used in this work.

To perform our analysis, for both α and β we consider the interval $[0.2, 5]$, while for J we consider the values from 2 to 11 (since $\lfloor \log_2(3075) \rfloor = 11$). The interval for α and β was selected in order to explore moderate deviations from the Shannon entropy, which is recovered in the limit $\alpha = \beta = 1$. Restricting the parameters to this range allows us to analyze how the Sharma–Mittal entropy varies around the Shannon case, while avoiding regimes corresponding to extreme parameter values where the entropy may display strongly non-Shannon behaviour. In this way, the comparison with the Shannon entropy remains meaningful and the resulting variations can be interpreted more clearly. To define the optimal grid resolution, we introduce a sensitivity analysis based on gradient and curvature distance measured on different grid resolutions. Let the wavelet Sharma–Mittal energy entropy measure be defined as a function of the parameters α, β, and the scale J, $S(\alpha, \beta, J)$. For each combination (α_i, β_j, J_k), the entropy value is evaluated on a discrete grid. Hence, the entropy surface can be represented as a three–dimensional function. To evaluate the effect of the grid resolution, we firstly compute distances of the gradient with respect to each dimension of the parameter space to compare the local variability of the surface according to a certain grid of dimension N. The corresponding measure is

$$D_1(S) = \frac{1}{N} \sum_{i,j,k} \sqrt{\left(\frac{\partial S}{\partial \alpha_i}\right)^2 + \left(\frac{\partial S}{\partial \beta_j}\right)^2 + \left(\frac{\partial S}{\partial J_k}\right)^2}$$

This distance reflects differences in the local slopes along each parameter direction.

Furthermore, we compute the distance on the second derivative, to assess the sensitivity of the grid granularity to the surface curvature

$$D_2(S) = \frac{1}{N}\sum_{i,j,k}\sqrt{\left(\frac{\partial^2 S}{\partial \alpha_i^2}\right)^2 + \left(\frac{\partial^2 S}{\partial \beta_j^2}\right)^2 + \left(\frac{\partial^2 S}{\partial J_k^2}\right)^2}$$

This distance captures discrepancies in the curvature and local smoothness of the entropy surfaces.

If these distances become negligible as the grid resolution increases, the entropy surface can be considered numerically stable with respect to the discretisation of (α, β). To achieve this, we compare the entropy surfaces computed on a coarse grid and on a finer grid using t test. Let $S^{(c)}(\alpha, \beta, J)$ the entropy evaluated on the coarse grid and $S^{(f)}(\alpha, \beta, J)$ the entropy evaluated on the fine grid, if the difference between $D_1(S^{(c)})$ and $D_1(S^{(f)})$ (or equivalently, $D_2(S^{(c)})$ and $D_2(S^{(f)})$) is not statistically significant, the coarse grid is preferred. Table 1 shows the results for grid resolution from 10 to 100 for both α and β.

Table 1. Surface gradient and curvature distances with p-values of t-tests between consecutive grid resolutions.

Grid	Brent				Platts				WTI			
	$D_1(S)$	$pD_1(S)$	$D_2(S)$	$pD_2(S)$	$D_1(S)$	$pD_1(S)$	$D_2(S)$	$pD_2(S)$	$D_1(S)$	$pD_1(S)$	$D_2(S)$	$pD_2(S)$
10	0.0985	-	0.0586	-	0.107	-	0.0698	-	0.0964	-	0.0522	-
20	0.0572	0.0001	0.0374	0.0005	0.0642	0.00007	0.0494	0.0034	0.0574	0.0003	0.0303	0.0001
30	0.0457	0.0009	0.0346	0.27	0.0520	0.0016	0.0469	0.44	0.0467	0.0030	0.0276	0.20
40	0.0407	0.016	0.0339	0.66	0.0467	0.028	0.0462	0.76	0.0421	0.036	0.0269	0.63
50	0.0381	0.076	0.0336	0.82	0.0438	0.113	0.0459	0.88	0.0396	0.131	0.0266	0.82
60	0.0365	0.177	0.0334	0.90	0.0420	0.232	0.0457	0.93	0.0382	0.258	0.0265	0.90
70	0.0354	0.29	0.0333	0.93	0.0409	0.35	0.0457	0.95	0.0372	0.38	0.0265	0.94
80	0.0347	0.393	0.0333	0.95	0.0401	0.453	0.0456	0.961	0.0366	0.481	0.0264	0.961
90	0.0342	0.481	0.0333	0.963	0.0395	0.536	0.0456	0.969	0.0361	0.564	0.0264	0.973
100	0.0338	0.554	0.0332	0.981	0.0391	0.604	0.0455	0.975	0.0358	0.629	0.0264	0.981

Table 1 shows that the average distances decrease as the grid resolution increases, indicating greater stability of the measure as the granularity increases. The p-values show that the differences between the coarser grids are statistically significant for gradients in most cases, while the differences in curvatures mainly become significant at the first grid transitions. Starting at 40×40, the p-values increase, suggesting that the differences between consecutive grids become negligible. To limit computational costs, we evaluate the differences between surfaces with a resolution $(\alpha, \beta, J) = (40 \times 40 \times 10)$. To provide a rough evaluation of the similarities in terms of price predictability in the various markets, we consider the surfaces $S_m, m = \{brent, dubai, wti\}$ of the calculated WSEEM, varying two out of three variables of the Ω space. Figures 2–4 show the results.

(**a**) (**b**)

Figure 2. Wavelet Sharma–Mittal Energy Entropy Measure of Brent crude oil futures prices: (**a**) as a function of J and β ($\alpha = 2.292$); (**b**) as a function of J and α ($\beta = 1.8$).

(**a**) (**b**)

Figure 3. Wavelet Sharma–Mittal energy entropy measure of WTI crude oil futures prices: (**a**) as a function of J and β ($\alpha = 2.292$); (**b**) as a function of J and α ($\beta = 1.8$).

(**a**) (**b**)

Figure 4. Wavelet Sharma–Mittal energy entropy measure of Dubai crude oil futures prices: (**a**) as a function of J and β ($\alpha = 2.292$); (**b**) as a function of J and α ($\beta = 1.8$).

Figures 2–4 illustrate two representative three-dimensional sections of the WSEEM surface for the Brent, WTI, and Dubai futures prices, respectively. Specifically, in Figures 2a, 3a and 4a, the parameter α is fixed, while the WSEEM is evaluated as a function of the wavelet scale J and the Sharma–Mittal parameter β. In particular, a similar monotonic dependence on parameter β can be highlighted. These aspects are also linked to the scale considered, with stability at low scales. For short time scales, corresponding to short-term horizons, the surface appears extremely flat and close to zero. This suggests that, in the short term, the measure is robust to variations in β and that the entropy of the system remains constant, with a predictable price dynamic while divergence emerges at high scales. As the resolution scale J increases, moving through a long-term behaviour, a sudden rise in the WSEEM value is observed, suggesting a greater impact of noise. Furthermore, can be noted that for lower β, WSEEM is greater for all levels J. In the Sharma–Mittal measure, β can be associated with the overall weighting of probabilities in the entropy measure, suggesting the co-existence of predictable factors of different natures, e.g., volatility clusters, long-range dependence and similar factors. The observed pattern indicates that lower values of β enhance the contribution of variability across scales, while higher values lead to a more uniform and less informative representation of the system dynamics.

However, relevant differences emerge across markets. The Brent surface appears smoother and more regular, with a gradual increase in WSEEM, suggesting a more stable and homogeneous dynamic. In contrast, WTI shows a steeper curve for extreme β, indicating higher sensitivity to the entropy parameters and a more reactive market behavior. Finally, the Dubai surface shows higher complexity for lower resolution scales, suggesting a greater role of noise in smaller time horizons.

Similarly, Figures 2b, 3b and 4b, the parameter β is fixed, while the WSEEM is evaluated as a function of the wavelet scale J and the Sharma–Mittal parameter α. In this case, a clear monotonic dependence on the parameter α emerges across all markets. The WSEEM increases as α increases, with a fast rise for low values followed by a progressive saturation

for higher α. This behavior reflects the role of α in controlling the global sensitivity of the Sharma–Mittal entropy, leading to a compression of differences as α increases. These features are strongly connected to the resolution scale J. At low scales, corresponding to short-term horizons, the surface remains relatively flat and close to zero for all values of α. This indicates that the measure is only weakly affected by variations in α, suggesting a stable and predictable price dynamic with limited informational divergence. As the scale J increases, a more pronounced dependence on α arises. For intermediate to large scales, the WSEEM exhibits a sharp increase for small values of α, followed by a clear plateau as α grows. This suggests that, in the long term, the system is more sensitive to structural differences, while the saturation effect indicates a loss of discrimination power at higher α levels. From an interpretative perspective, α measures the importance of the tails in the probability distribution. Also, in this case, relevant differences emerge across markets. The Brent surface appears smoother, with a more gradual transition from growth to saturation, suggesting a more stable and homogeneous dynamic across scales. WTI exhibits a steeper initial increase in α, indicating a stronger sensitivity to parameter variations, particularly at medium and high scales. Finally, the Dubai surface shows the most pronounced nonlinearity, with a rapid rise and early saturation, pointing to a more complex and less regular structure, especially in the transition from short- to long-term dynamics. Although noticeable differences arise in terms of the absolute entropy values and the precise location of local extrema, the overall geometry of the surfaces remains invariant across markets. In particular, all three benchmarks display:

1. A scale–dependent maximum of entropy;
2. A monotonic response to the parameter β;
3. A tendency toward saturation for extreme values of the entropic parameters.

These findings provide evidence of strong cross-market similarities in the multiscale organization of crude oil futures prices. The observed invariance suggests that the mechanisms governing the loss and recovery of predictability are largely shared across different oil benchmarks, pointing to a common underlying market structure driven by global information flows and synchronized trading activity. Consequently, the WSEEM emerges as a robust and informative tool for jointly characterizing the predictability and cross-market complexity in crude oil markets.

4.2. Cross-Market Effects Evaluation

To evaluate the cross-market effects of crude oil, we propose the following measures of the discrepancy in WSEEM. Let S_l and S_m denote the $WSEEM_{\alpha,\beta,J}$ surfaces over the (α, β, J) grid for $l, m = \{brent, wti, dubai\}$. For each combination in the support $\Omega \subset \mathbb{R}^3$, we quantify similarity using the Pearson correlation of the surfaces

$$\rho WSEEM(S_l, S_m) = \frac{\int_\Omega \left(S_l(\alpha,\beta,J) - \overline{S}_l\right)\left(S_m(\alpha,\beta,J) - \overline{S}_m\right) d\alpha\, d\beta\, dJ}{\sqrt{\int_\Omega \left(S_l(\alpha,\beta,J) - \overline{S}_l\right)^2 d\alpha\, d\beta\, dJ}\ \sqrt{\int_\Omega \left(S_m(\alpha,\beta,J) - \overline{S}_m\right)^2 d\alpha\, d\beta\, dJ}},$$

where $\overline{S}_l = \frac{1}{|\Omega|}\int_\Omega S_l(\alpha,\beta,J)\, d\alpha\, d\beta\, dJ$;

The L_2 distance is

$$L_2 WSEEM(S_l, S_m) = \sqrt{\int_\Omega \left(S_l(\alpha,\beta,J) - S_m(\alpha,\beta,J)\right)^2 d\alpha\, d\beta\, dJ}$$

and the Kendall rank concordance is

$$\tau WSEEM(S_l, S_m) = \frac{2}{|\Omega|^2 - |\Omega|} \int_\Omega \int_\Omega \operatorname{sgn}\left(S_l(\alpha, \beta, J) - S_l(\alpha', \beta', J')\right) \cdot \operatorname{sgn}\left(S_m(\alpha, \beta, J) - S_m(\alpha', \beta', J')\right) d\alpha\, d\beta\, dJ\, d\alpha'\, d\beta'\, dJ'.$$

We also introduce the following discrepancy measures to determine the difference in terms of surface shape.

$$\Delta WSEEM_{\text{abs}}(S_l, S_m) = \frac{1}{|\Omega|} \int_\Omega \left|S_l(\alpha, \beta, J) - S_m(\alpha, \beta, J)\right| d\alpha\, d\beta\, dJ,$$

$$\Delta WSEEM_{\text{rel}}(S_l, S_m) = \frac{1}{|\Omega|} \int_\Omega \frac{\left|S_l(\alpha, \beta, J) - S_m(\alpha, \beta, J)\right|}{\frac{1}{2}\left(S_l(\alpha, \beta, J) + S_m(\alpha, \beta, J)\right)} d\alpha\, d\beta\, dJ,$$

To quantify the robustness of the similarity measures, we implement a Moving Block Bootstrap procedure along the time dimension. For a time block of length L, let $\{p_t\}_{t=1}^{T}$ denote the underlying log-price series used to compute $WSEEM_{\alpha,\beta}$. For each bootstrap replication $b = 1, \ldots, B$, we construct a pseudo–sample by randomly drawing with replacement $\lceil T/L \rceil$ from the original series and concatenating them until reaching length T. For each bootstrap sample, we recompute the $WSEEM_{\alpha,\beta}$ surface and the associated similarity metrics $(\rho WSEEM, L_2WSEEM, \tau WSEEM, \Delta WSEEM_{abs}, \Delta WSEEM_{rel})$. Confidence intervals for the similarity measures are then obtained from the empirical distribution of the bootstrap estimates. To enable us to capture trend-cycle dynamics in log-prices, we define $L = 40$, about two trading months, for a total of approximately 3000 blocks, to calculate $B = 100$ bootstrap replicates. Table 2 shows the results.

Table 2. Bootstrap indices estimates with 95% confidence intervals.

Index	Series 1	Series 2	Mean	Lower (2.5%)	Upper (97.5%)
$\rho WSEEM$	Brent	Dubai	0.9997	0.9989	0.9999
	Brent	WTI	0.9998	0.9995	0.9999
	Dubai	WTI	0.9995	0.9987	0.9999
$\tau WSEEM$	Brent	Dubai	0.9854	0.9709	0.9934
	Brent	WTI	0.9897	0.9804	0.9958
	Dubai	WTI	0.9823	0.9640	0.9923
L_2WSEEM	Brent	Dubai	0.8330	0.4105	1.4859
	Brent	WTI	0.5891	0.2501	1.0482
	Dubai	WTI	1.0699	0.5015	1.9169
$\Delta WSEEM_{abs}$	Brent	Dubai	0.0037	0.0018	0.0070
	Brent	WTI	0.0026	0.0011	0.0048
	Dubai	WTI	0.0048	0.0021	0.0095
$\Delta WSEEM_{rel}$	Brent	Dubai	0.0554	0.0250	0.1028
	Brent	WTI	0.0386	0.0180	0.0716
	Dubai	WTI	0.0720	0.0289	0.1353

Specifically, Table 2 shows the bootstrap estimates of the dependence measures and surface differences among the three price series pairs: Brent–Dubai, Brent–WTI, and Dubai–WTI. In particular, for Pearson correlation $\rho WSEEM$, all pairs exhibit extremely high correlation. The Brent–WTI pair has the highest, followed closely by Brent–Dubai, and Dubai–WTI. The small confidence intervals suggests that the correlations are robust, confirming almost perfect linear co-movement among these benchmarks. Similarly, rank correlations $\tau WSEEM$ are very high, reflecting strong monotonic relationships. Brent–WTI

shows the strongest association, while Dubai–WTI exhibits slightly lower dependence. This suggests that while all series move together, Brent and WTI are the most consistently aligned in their relative rankings. The L_2WSEEM measure captures point-by-point distance between the surfaces. Brent–WTI has the smallest, indicating very similar WSEEM behavior. Brent–Dubai shows moderate differences, whereas Dubai–WTI exhibits the largest, reflecting greater discrepancy in WSEEM surface shapes. $\Delta WSEEM_{abs}$ quantifies the average absolute difference between surfaces. Brent–WTI has the lowest value, confirming the close alignment of prices. Brent–Dubai and Dubai–WTI show larger absolute deviations, consistent with the L_2 distance results. $\Delta WSEEM_{abs}$ considers the surface discrepancy in proportion to their magnitude, but results are almost similar to the absolute measure. Brent–WTI remains the closest pair, while Dubai–WTI shows the highest relative deviations. This highlights that, proportionally, Dubai differs more from WTI than Brent does. Overall, these indices consistently show that Brent and WTI prices are the closest in WSEEM behavior, both linearly and in surface shape, while Dubai introduces slightly larger deviations. The narrow bootstrap confidence intervals across all indices indicate that these estimates are statistically stable, and the results provide a comprehensive scenario of both linear dependence and functional similarity among the three benchmark series.

Furthermore, to statistically evaluate the divergence with respect to the average, perform a functional ANOVA (fANOVA) over the (α, β, J) grid to formally test whether the surfaces differ systematically across market benchmarks. Let $S_m(\alpha_i, \beta_j, J_k)$ denote the value of the $WSEEM_{\alpha,\beta}$ surface for market $m \in \{brent, wti, dubai\}$ at grid point (α_i, β_j, J_k). We consider the functional decomposition

$$S_b(\alpha_i, \beta_j, J_k) = \mu(\alpha_i, \beta_j, J_k) + \gamma_m(\alpha_i, \beta_j, J_k) + \varepsilon_{b,i,j,k},$$

where $\mu(\alpha_i, \beta_j, J_k)$ represents the mean surface across markets and $\gamma_m(\alpha_i, \beta_j, J_k)$ captures the market–specific deviation from the mean surface. Under the null hypothesis of surface similarity, we have

$$H_0 : \gamma_m(\alpha_i, \beta_j, J_k) = 0 \quad \forall m, i, j, k.$$

We perform fANOVA with 30 random projections and 100 bootstrap repetitions. Table 3 shows the results.

Table 3. Functional ANOVA with Bonferroni and FDR procedures and a confidence level of 0.95.

	Test Bonferroni			**Test FDR**		
	Alpha	**Beta**	**J**	**Alpha**	**Beta**	**J**
p-value	$\ll 0.01$	$\ll 0.01$	$\ll 0.01$	$\ll 0.01$	$\ll 0.01$	$\ll 0.01$

Table 3 shows that it is possible to reject H_0 for all the grid-variables α, β, and J, implying that the curves of the three markets are not identical point-by-point. This suggests the existence of market-specific effects on entropy dynamics. However, analysis of the similarity indices confirms that these differences are very small, as evidenced by the similarity indices, suggesting the existence of co-movements across markets.

4.3. Effects of Shocks on WSEEM Behaviour

To investigate the time-varying reliability of the proposed WSEEM measure, we implement a rolling window analysis on daily price series. Let $\{p_t\}_{t=1}^{T}$ denote the underlying log-price series used ot compute WSEEM. For a given window size W, overlapping subsamples $p_t, \ldots, p_{t+W-1}$, with $t = 1, 1+h, 1+2h, \ldots$, where h denotes the horizon between consecutive windows. We set a temporal window of $W = 180$ observations, corresponding to approximately six months of trading data, and a horizon of $h = 10$, corresponding

to two trading weeks. This choice balances the need to capture medium-term dynamics while reducing computational burden and smoothing short-term fluctuations. For the sake of simplicity, we compute the average WSEEM across α, β, and J, maintaining the original grid $40 \times 40 \times \max(J)$. Figure 5 shows the resulting time series of WSEEM values, aligned with the ending date of each rolling window, and highlighting different regimes corresponding to major disruptions in the oil market, namely the 2014–2015 supply shock, the 2020 COVID-19 pandemic, and the 2022 geopolitical shock. This framework enables us to evaluate whether the entropy geometry remains stable across regimes or exhibits systematic deviations associated with periods of market crisis.

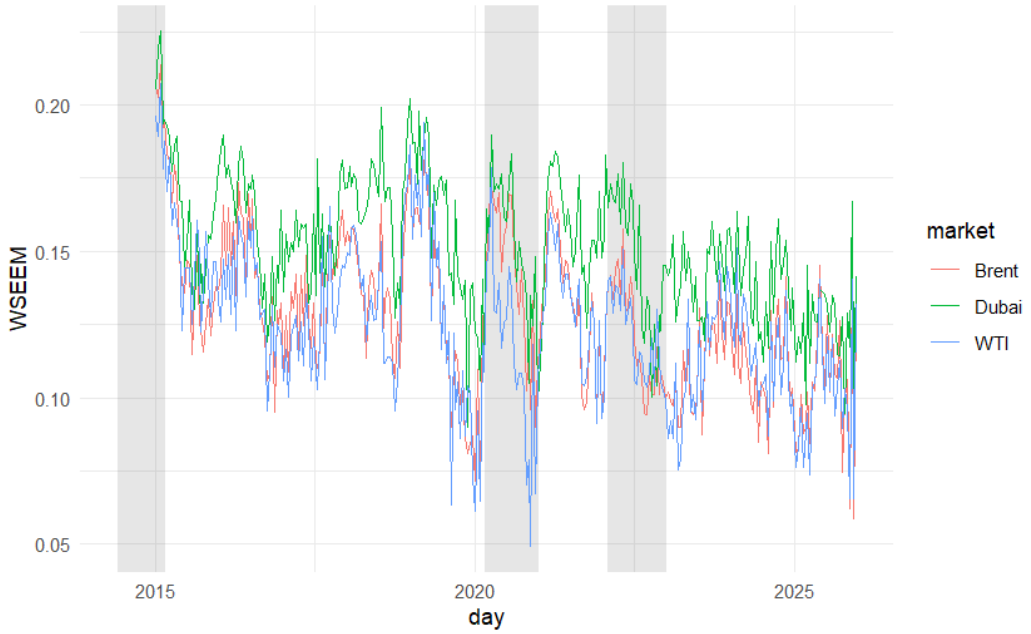

Figure 5. Average WSEEM estimation across time, compared to the main oil crisis in 2014–2025.

Figure 5 shows that WTI, Brent, and Dubai entropy dynamics have a highly synchronized baseline pattern, indicating substantial informational integration across global oil markets. Despite this overall alignment, systematic differences emerge: Dubai exhibits consistently higher entropy and lower predictability, WTI shows lower baseline entropy but higher volatility and susceptibility to shocks, while Brent lies between the two. During periods of market stress, deviations from the baseline are pronounced. The 2014–2015 supply shock is characterised by initially elevated WSEEM values, reflecting strong multiscale disorganisation, followed by rapid system reorganization and cross-market re-synchronisation. The 2020 pandemic episode presents the most noticeable divergence: WTI entropy drops strongly, significantly more than Brent and Dubai, highlighting market-specific frictions likely related to storage constraints and negative futures pricing. This suggests a temporary breakdown in the usual entropy geometry and cross-market integration. In contrast, the 2022 geopolitical shock, while increasing overall volatility, maintains a higher degree of alignment among the three series, consistent with a more symmetric global shock and the absence of idiosyncratic market frictions. Long-term trends indicate a modest decrease in entropy over time, with WSEEM peaking during 2014–2016 and declining thereafter, potentially reflecting increased market efficiency, enhanced informational integration, or structural changes in market micro-structure. Overall, these results strengthens the hypothesis that, while the entropy geometry is broadly stable across oil markets, significant market-specific characteristics exist and emerge during episodes of extreme stress. In particular, the 2020 WTI divergence provides compelling evidence of market-specific constraints,

whereas other shocks tend to preserve the integrated structure, supporting the view of a largely coherent global oil market.

5. Conclusions

In this paper we analyse the multi-scale informational structure of major crude oil benchmarks, Brent, WTI, and Dubai, through a measure that combines wavelet with entropy, namely the Wavelet Sharma–Mittal Energy Entropy Measure. By jointly varying the entropic parameters and the wavelet scale, we provide a unified framework for assessing the predictability of the three oil benchmarks across both markets and time horizons.

A remarkable structural regularity is revealed by the empirical data. Despite variations in entropy magnitude among benchmarks, the WSEEM surfaces' geometry is remarkably stable. The scale dependence, sensitivity to the entropic parameters, and transitions between higher and lower predictability regimes are similar across all markets. This invariance implies that the multi-scale complexity architecture of crude oil benchmarks is similar.

The discrepancy analysis further indicates that cross-market differences are localised and parameter, and contingent rather than systemic. Deviations concentrate at intermediate scales and for low values of the entropic parameters, particularly where the entropy functional emphasises the global dispersion of the energy distribution. Outside these regions, the entropy landscapes converge, reinforcing the idea of a shared structural organization.

All of these results suggest that crude oil benchmarks have a high level of information integration. The multi-scale structure of price dynamics is not significantly changed by regional traits or liquidity conditions, although they may have an impact on the degree of predictability. In this sense, oil markets appear to differ in magnitude but not in structural complexity. These findings are consistent with evidence stating that futures markets, particularly for WTI, play a leading role in incorporating new information into spot prices [32,33]. Furthermore, the relationships between spot and futures are often complex and non-linear, as analysed by [34]. Furthermore, the findings of structurally similar multi-scale entropy patterns across Brent, WTI, and Dubai enhance existing evidence on inter-market interactions, such as volatility spillovers between WTI and Brent spot prices [35,36]. The Dubai benchmark, historically pivotal in shaping oil pricing for Middle Eastern exports to Asia [37], provides additional context for understanding cross-market information integration. While spillover studies focus on transmission of risk and short-term dependencies, the WSEEM framework provides a more comprehensive interpretation of the informational structure and predictability across scales, detecting a common multi-scale complexity among oil markets.

Broadly speaking, the results highlight the usefulness of generalised entropy measures in capturing subtle but economically meaningful differences in multi-scale predictability. The WSEEM framework is a versatile tool for studying informational efficiency in globally integrated commodity markets since it can distinguish between structural similarities and localized deviations.

The proposed WSEEM framework presents several methodological strengths. First, it integrates multiscale decomposition with a generalized entropy formulation, allowing for a flexible and parameter-sensitive assessment of predictability. Second, it captures both structural similarities and localized deviations across markets, providing a richer perspective than single-scale or single-parameter entropy measures. Finally, its discrepancy analysis offers a transparent way to evaluate cross-market integration beyond standard correlation-based metrics.

Nevertheless, some limitations should be acknowledged. The measure depends on the selection of entropic parameters and the wavelet decomposition scheme, which may

influence quantitative results. Although the qualitative patterns observed in this study appear robust, future research could explore data-driven parameter selection procedures or alternative wavelet bases. Moreover, WSEEM does not provide direct information about the underlying data-generating process or identify specific predictive models, but instead captures deviations from a white-noise benchmark in the time–frequency domain. Finally, the present analysis focuses on crude oil futures markets; extending the framework to other commodities, financial assets, or periods characterized by structural breaks would help assess its broader applicability.

As an entropy-based measure, WSEEM has a direct interpretation in terms of predictability. When energy is concentrated at specific scales, the process exhibits structured temporal dependence, implying that past observations may contain information about future dynamics. Conversely, when energy is more evenly distributed across scales, the process resembles white noise, suggesting limited or no exploitable information in past observations. In this sense, WSEEM can be interpreted as a time–frequency measure of deviation from a white-noise benchmark, and therefore as a proxy for the degree of potential predictability embedded in the signal.

A rigorous assessment of predictability would require an extensive model selection exercise across a wide range of specifications, including deterministic components (e.g., trigonometric regressions and outlier adjustments), heteroskedastic models (e.g., HAR or GARCH families), linear models (e.g., ARIMA), long-memory processes, and nonlinear approaches (e.g., threshold models or neural networks). Restricting the analysis to a limited subset of models may lead to incomplete or potentially misleading conclusions, particularly given that real-world time series often exhibit nonlinear dynamics, structural breaks, and deterministic shocks associated with major events.

Future research may build on these aspects by investigating dynamic or rolling implementations of WSEEM to analyze time-varying predictability, as well as its integration with forecasting frameworks. An interesting direction would be to explore the relationship between WSEEM dynamics and the performance of different classes of predictive models in order to assess whether variations in entropy-based measures are systematically associated with changes in model-specific forecasting ability. Such extensions could provide deeper insights into the evolution of informational efficiency in globally integrated markets.

Therefore, the proposed measure should be interpreted as an indicator of potential predictability, capturing deviations from white-noise behavior in the time–frequency domain without imposing assumptions on the underlying data-generating process or restricting attention to a specific class of models.

Author Contributions: All authors contributed equally to the article. All authors have read and agreed to the published version of the manuscript.

Funding: This research received no external funding.

Data Availability Statement: Data was retrieved on public database investing.com.

Acknowledgments: Maria Carannante and Alessandro Mazzoccoli are members of the INdAM Research group GNCS.

Conflicts of Interest: The authors declare no conflicts of interest.

References

1. Kilian, L. Oil price shocks: Causes and consequences. *Annu. Rev. Resour. Econ.* **2014**, *6*, 133–154. [CrossRef]
2. Caporin, M.; Fontini, F.; Talebbeydokhti, E. Testing persistence of WTI and Brent long-run relationship after the shale oil supply shock. *Energy Econ.* **2019**, *79*, 21–31. [CrossRef]
3. Imsirovic, A. The Trading and Price Discovery for Crude Oils. In *The Palgrave Handbook of International Energy Economics*; Springer International Publishing: Cham, Switzerland, 2022; pp. 327–358. [CrossRef]

4. Fattouh, B. The dynamics of crude oil price differentials. *Energy Econ.* **2010**, *32*, 334–342. [CrossRef]
5. IPCC. *2006 IPCC Guidelines for National Greenhouse Gas Inventories, Volume 2: Energy*; IPCC: Hayama, Japan, 2006.
6. Mann, J.; Sephton, P. Global relationships across crude oil benchmarks. *J. Commod. Mark.* **2016**, *2*, 1–5. [CrossRef]
7. Liu, W.M.; Schultz, E.; Swieringa, J. Price dynamics in global crude oil markets. *J. Futur. Mark.* **2015**, *35*, 148–162. [CrossRef]
8. Charles, A.; Darné, O. The efficiency of the crude oil markets: Evidence from variance ratio tests. *Energy Policy* **2009**, *37*, 4267–4272. [CrossRef]
9. Kang, S.H.; Lee, J. Time-varying market efficiency in the Brent and WTI crude oil markets. *Financ. Res. Lett.* **2022**, *46*, 102339.
10. Elder, J.; Miao, H.; Ramchander, S. Price discovery in crude oil futures. *Energy Econ.* **2014**, *46*, S18–S27. [CrossRef]
11. Zhang, Z.; Raza, M.Y.; Wang, W.; Sui, L. Volatility predictability in crude oil futures: Evidence based on OVX, GARCH and stochastic volatility models. *Energy Strategy Rev.* **2023**, *50*, 101209. [CrossRef]
12. Balcilar, M.; Demirer, R.; Gupta, R. OPEC news and predictability of oil futures returns and volatility: Evidence from a nonparametric causality-in-quantiles approach. *N. Am. J. Econ. Financ.* **2018**, *45*, 123–144.
13. Balcilar, M.; Gupta, R.; Pierdzioch, C. Predictability of crude oil prices: An investor perspective. *Energy Econ.* **2018**, *74*, 130–142.
14. Mastroeni, L.; Mazzoccoli, A.; Vellucci, P. Dynamic time warping for the analysis of energy commodity price dynamics. *Energy Econ.* **2021**, *95*, 105104.
15. Ajmi, A.N.; Hammoudeh, S.; Mokni, K. Detection of bubbles in WTI, brent, and Dubai oil prices: A novel double recursive algorithm. *Resour. Policy* **2021**, *70*, 101956. [CrossRef]
16. Phillips, P.C.; Shi, S.P. Financial bubble implosion and reverse regression. *Econom. Theory* **2018**, *34*, 705–753. [CrossRef]
17. Keerthan, J.S.; Nagasai, Y.; Shaik, S. Machine learning algorithms for oil price prediction. *Int. J. Innov. Technol. Explor. Eng. (IJITEE)* **2019**, *8*, 958–963.
18. Gupta, N.; Nigam, S. Crude oil price prediction using artificial neural network. *Procedia Comput. Sci.* **2020**, *170*, 642–647. [CrossRef]
19. Doroshenko, L.; Mastroeni, L.; Mazzoccoli, A. Wavelet and Deep Learning Framework for Predicting Commodity Prices Under Economic and Financial Uncertainty. *Mathematics* **2025**, *13*, 1346. [CrossRef]
20. Mastroeni, L.; Mazzoccoli, A.; Vellucci, P. Studying the impact of fluctuations, spikes and rare events in time series through a wavelet entropy predictability measure. *Phys. A Stat. Mech. Its Appl.* **2024**, *641*, 129720. [CrossRef]
21. Mastroeni, L.; Mazzoccoli, A.; Vellucci, P. Wavelet entropy and complexity–entropy curves approach for energy commodity price predictability amid the transition to alternative energy sources. *Chaos Solitons Fractals* **2024**, *184*, 115005. [CrossRef]
22. Mastroeni, L.; Mazzoccoli, A. Quantifying predictive knowledge: Wavelet energy α-divergence measure for time series uncertainty reduction. *Chaos Solitons Fractals* **2024**, *188*, 115488. [CrossRef]
23. Mazzoccoli, A. Assessing time series predictability by extending wavelet energy-based entropy and divergence measures using the Sharma–Mittal framework. *Chaos Solitons Fractals* **2025**, *201*, 117351. [CrossRef]
24. Christensen, O. An introduction to wavelet analysis. In *Functions, Spaces, and Expansions: Mathematical Tools in Physics and Engineering*; Springer: Berlin/Heidelberg, Germany, 2010; pp. 159–180.
25. Doroshenko, L.; De Crescenzo, I.; Mastroeni, L.; Mazzoccoli, A. Geopolitical risks, critical materials and energy transition: Insights from wavelet analysis. *Resour. Policy* **2025**, *108*, 105666. [CrossRef]
26. Mallat, S.G. A theory for multiresolution signal decomposition: The wavelet representation. *IEEE Trans. Pattern Anal. Mach. Intell.* **2002**, *11*, 674–693. [CrossRef]
27. Alvarez-Ramirez, J.; Espinosa-Paredes, G.; Vernon-Carter, E.J. Causal wavelet analysis of the Bitcoin price dynamics. *Phys. A Stat. Mech. Its Appl.* **2025**, *658*, 130307. [CrossRef]
28. Zhang, Z. The improvement of the discrete wavelet transform. *Mathematics* **2023**, *11*, 1770. [CrossRef]
29. Kayid, M.; Alshehri, M.A. Tsallis entropy for the past lifetime distribution with application. *Axioms* **2023**, *12*, 731. [CrossRef]
30. Kolesnichenko, A. Two-Parameter Sharma–Mittal Entropy Functional as the Foundation of the Family of Generalized Thermodynamics of Nonextensive Systems. *Sol. Syst. Res.* **2025**, *59*, 15. [CrossRef]
31. Jäckle, S.; Keller, K. Tsallis entropy and generalized Shannon additivity. *Axioms* **2017**, *6*, 14. [CrossRef]
32. Silvapulle, P.; Moosa, I.A. The relationship between spot and futures prices: Evidence from the crude oil market. *J. Futur. Mark.* **1999**, *19*, 175–193. [CrossRef]
33. Zavadska, M.; Morales, L.; Coughlan, J. The Lead–Lag Relationship between Oil Futures and Spot Prices—A Literature Review. *Int. J. Financ. Stud.* **2018**, *6*, 89. [CrossRef]
34. Bekiros, S.D.; Diks, C.G. The relationship between crude oil spot and futures prices: Cointegration, linear and nonlinear causality. *Energy Econ.* **2008**, *30*, 2673–2685. [CrossRef]
35. Atukeren, E.; Çevik, E.İ.; Korkmaz, T. Volatility spillovers between WTI and Brent spot crude oil prices: An analysis of granger causality in variance patterns over time. *Res. Int. Bus. Financ.* **2021**, *56*, 101385. [CrossRef]

36. Ren, X.; He, Y.; Liu, C.; Tao, L. Extreme risk spillovers between SC, WTI and Brent crude oil futures: Evidence from time-varying Granger causality test. *Energy* **2025**, *320*, 135495. [CrossRef]
37. Fattouh, B. Oil price benchmarks in international trade: The Dubai benchmark and its role in the international oil pricing system. *Oxf. Energy Forum* **2012**, *87*, 17–19.